Path-integral computation of superfluid densities

E. L. Pollock and D. M. Ceperley
Lawrence Livermore National Laboratory, University of California, Livermore, California 94550
(Received 9 July 1987)

The normal and superfluid densities are defined by the response of a liquid to sample boundary motion. The free-energy change due to uniform boundary motion can be calculated by path-integral methods from the distribution of the winding number of the paths around a periodic cell. This provides a conceptually and computationally simple way of calculating the superfluid density for any Bose system. The linear-response formulation relates the superfluid density to the momentum-density correlation function, which has a short-ranged part related to the normal density and, in the case of a superfluid, a long-ranged part whose strength is proportional to the superfluid density. These facts are discussed in the context of path-integral computations and demonstrated for liquid ^{4}He along the saturated vapor-pressure curve. Below the experimental superfluid transition temperature the computed superfluid fractions agree with the experimental values to within the statistical uncertainties of a few percent in the computations. The computed transition is broadened by finite-sample-size effects.

I. INTRODUCTION

It has been recently demonstrated that the microscopic properties of interacting Bose systems can be calculated by discretized-path-integral computations of the density matrix.[1,2] Most laboratory examples of superfluidity are, however, best described by two-fluid hydrodynamics. The connection between the microscopic description and the two-fluid model and, in particular, determination of the superfluid density, can be made by considering the system response to sample boundary motion. The free-energy change in a periodic system is related to the path-integral winding number, while the linear-response function is the momentum-density correlation function (MDCF).[3] In this article these relations are presented and discussed in a form useful in path-integral computations. Path-integral simulation results for liquid[4] He at temperatures above and below the λ transition are then used as an illustration. While the values obtained, so far, for the superfluid densities of ^{4}He along the saturated-vapor-pressure (SVP) curve from these simulations are numerically not more precise than the Landau formula which relates the superfluid fraction to the experimentally determined excitation spectrum, these simulations use as input only the interparticle potential, $\hbar$, and the mass of the helium atom, and provide information not given by quasi-particle approximations. These simulation methods have previously been used to calculate the momentum condensate and the specific heat in ^{4}He.[2]

II. PATH-INTEGRAL COMPUTATIONS OF THE DENSITY MATRIX

All of the statistical-mechanical properties of a many-body system may be determined from the density matrix

$$\rho(R,R';\beta)=\langle R \mid e^{-\beta H} \mid R' \rangle = \sum_n e^{-\beta E_n}\Psi_n(R)\Psi_n(R') , \tag{1}$$

where the summation is over energy eigenstates of the system and $\beta=1/k_BT$. In particular, the next section discusses how the superfluid density may be obtained from the density matrix, so it is necessary to first discuss how it is computed.

The basic identity for discretized-path-integral computations of the density matrix is

$$\rho(R,R';\beta)= \int \rho(R,R_1;\tau)\rho(R_1,R_1;\tau)\cdots\rho(R_{M-1},R';\tau) \times dR_1\cdots dR_{M-1} , \tag{2}$$

where $\tau\equiv\beta/M$ for some positive integer M and the R variables denote points in the $3N$-dimensional coordinate space. The $R,R_1,R_2,\ldots,R'$ in this equation describe the discretized paths of the particles. Each step in the path is associated with a high-temperature density matrix. The advantage in using this identity is that, for sufficiently large M (small τ), an accurate approximation for the high-temperature density matrices is known. The best convenient approximation is the pair-product form

$$\rho(R,R';\tau)= \prod_{i=1}^{N}\rho_1(\mathbf{r}_i,\mathbf{r}_i';\tau) \prod_{\substack{i,j=1\\ i<j}}^{N} \exp[-U(\mathbf{r}_{ij},\mathbf{r}_{ij}';\tau)] , \tag{3}$$

where the one-particle, or ideal-gas term,

$$\rho_1(\mathbf{r}_i,\mathbf{r}_i';\tau)= \left[\frac{m}{2\pi\hbar^2\tau}\right]^{3/2} \exp\left[-\frac{(\mathbf{r}_i-\mathbf{r}_i')^2}{2\hbar^2\tau/m}\right] , \tag{4}$$

and U gives the nonideal part of the pair density matrix

obtained by solving the two-particle Bloch equation. Equation (3) becomes exact as τ decreases. The corrections are of order τ^3.

For periodic boundary conditions Eqs. (3) and (4) must include sums over the periodic images. The one-particle term is then

$$\rho_1(\mathbf{r}_i,\mathbf{r}_i';\tau)=\sum_{\mathbf{L}}\left[\frac{m}{2\pi\hbar^2\tau}\right]^{3/2}\exp\left[-\frac{(\mathbf{r}_i-\mathbf{r}_i'+\mathbf{L})^2}{2\hbar^2\tau/m}\right], \tag{5}$$

where the $\mathbf{L}$ are periodic lattice vectors.

In applying these formulas to Bose systems, an additional sum over permutations is necessary to symmetrize the density matrix,

$$\rho_{\text{Bose}}(R,R';\beta)=\frac{1}{N!}\sum_{\mathcal{P}}\rho(R,\mathcal{P}R';\beta)\ . \tag{6}$$

Without permutations, the path for each particle will repeat after M steps, for $R=R'$. With permutations, a path can involve many particles and steps before repeating, depending on the cyclic structure of the permutation. In the computations the permutations $\mathcal{P}$ and the path variables $R_1,\ldots,R_M$ are sampled by a generalized Metropolis algorithm. Some computational details are given in Ref. 2.

At high temperatures only the identity permutation contributes significantly to this sum, but at lower temperatures—such that the de Broglie thermal wavelength becomes comparable to the interparticle spacing—other permutations also become important. In particular, it is the long cyclic permutations that are essential both for Bose condensation and superfluidity. These effects are due to the one particle terms, Eq. (4), modified by the interaction. For the ideal Bose gas only particles on the same permutation cycle are correlated in $\rho(R,\mathcal{P}R';\beta)$.

III. CALCULATION OF ρ_s

A. Relationship to the winding number

The normal and superfluid components are experimentally determined by their different response to boundary motion. The *Gedanken* experiment envisioned here corresponds to a system enclosed between two cylinders of radii R and $R+d$ rotating with angular frequency ω. For $d/R\ll 1$ the centrifugal effects can be neglected and the system becomes equivalent to one enclosed between two planes moving with velocity $\omega R=v$ but periodic in one direction. The density matrix for a system with moving walls, $\rho_{\mathbf{v}}$, is needed to calculate this response.[4] The density-matrix operator for this system can be immediately written down in a frame at rest with the boundary walls (primed frame) as

$$\rho'=e^{-\beta H'}\ , \tag{7}$$

where

$$H'=\sum_j\frac{(\mathbf{p}_j-m\mathbf{v})^2}{2m}+V\ , \tag{8}$$

with V representing the particle interactions. This scalar operator is unchanged in going to the lab frame (in physical terms the distribution of states is identical in the lab and moving frames), so $\rho_{\mathbf{v}}=\rho'$.

Defining the normal component of the fluid as that part which responds to this boundary motion,

$$\frac{\rho_N}{\rho}Nm\mathbf{v}=\langle\mathbf{P}\rangle_{\mathbf{v}}=\frac{\text{Tr}[\mathbf{P}\rho_{\mathbf{v}}]}{\text{Tr}[\rho_{\mathbf{v}}]}\ , \tag{9}$$

where $\mathbf{P}$ is the total momentum. Expanding $\rho_{\mathbf{v}}$ to first order in $\mathbf{v}$ will give an expression for ρ_N in terms of the momentum-density correlations.[3] This approach will be discussed in the next subsection. In terms of the free energy for the system with moving walls,

$$e^{-\beta F_v}=\text{Tr}[\rho_{\mathbf{v}}]\ , \tag{10}$$

Eq. (9) may be rewritten as

$$\frac{\rho_N}{\rho}Nm\mathbf{v}=\frac{\partial}{\beta\partial\mathbf{v}}\ln(\text{Tr}[\rho_{\mathbf{v}}])+Nm\mathbf{v}=-\frac{\partial F_v}{\partial\mathbf{v}}+Nm\mathbf{v}\ , \tag{11}$$

or

$$\frac{\rho_S}{\rho}=\frac{\partial(F_v/N)}{\partial(\frac{1}{2}mv^2)}\ . \tag{12}$$

The free-energy change due to the motion of the sample walls is thus

$$\frac{\Delta F_v}{N}=\tfrac{1}{2}mv^2\frac{\rho_S}{\rho}+O(v^4)\ . \tag{13}$$

When there is no superfluid present, the free energy is unaffected by uniform boundary motion. This is clearly true for any classical system. The experimental ρ_S values are for the limit $v\to 0$ and ρ_S will here after refer to this limit.

The path-integral algorithm can be easily modified to compute $\rho_{\mathbf{v}}$ and ΔF_v. From Eqs. (7) and (8), $\rho_{\mathbf{v}}$ satisfies the Bloch equation

$$-\frac{\partial\rho_{\mathbf{v}}(R,R';\beta)}{\partial\beta}=\left[\frac{1}{2m}\sum_j(-i\hbar\nabla_j-m\mathbf{v})^2+V\right]\times\rho_{\mathbf{v}}(R,R';\beta)\ , \tag{14}$$

with periodic boundary conditions,

$$\rho_{\mathbf{v}}(r_1,\ldots,r_N,r_1',\ldots,r_j'+\mathbf{L},\ldots,r_N';\beta)=\rho_{\mathbf{v}}(r_1,\ldots,r_N,r_1',\ldots,r_N';\beta)\ . \tag{15}$$

Define $\tilde{\rho}$ by

$$\rho_{\mathbf{v}}(R,R';\beta)=\exp\left[i\frac{m}{\hbar}\mathbf{v}\cdot\sum_j(\mathbf{r}_j-\mathbf{r}_j')\right]\tilde{\rho}(R,R';\beta)\ , \tag{16}$$

and note

$$e^{-\beta F_{\mathbf{v}}}=\text{Tr}[\tilde{\rho}]\ . \tag{17}$$

$\tilde{\rho}$ satisfies the usual Bloch equation for a system with stationary walls,

$$-\frac{\partial\tilde{\rho}(R,R';\beta)}{\partial\beta}=\left[\frac{1}{2m}\sum_j(-i\hbar\nabla_j)^2+V\right]\tilde{\rho}(R,R';\beta)\ , \tag{18}$$

but behaves under periodic translations as

$$\tilde{\rho}(r_1,\ldots,r_N,r_1',\ldots,r_j'+\mathbf{L},\ldots,r_N';\beta)=\exp\left[i\frac{m}{\hbar}\mathbf{v}\cdot\mathbf{L}\right]\tilde{\rho}(r_1,\ldots,r_N,r_1',\ldots,r_N';\beta)\ .$$

Hence we can use the usual density matrix for a system with stationary walls to calculate $\rho_{\mathbf{v}}$ if the phase factor is included as a weight. In particular, in a path-integral calculation the contribution to the density matrix from a path ending on a periodic image of its initial point must include the $e^{i(m/\hbar)\mathbf{v}\cdot\mathbf{L}}$ factor. This is most easily done by defining the winding number, $\mathbf{W}$, by

$$\sum_{i=1}^{N}(\mathbf{r}_{\mathcal{P}_i}-\mathbf{r}_i)=\mathbf{W}L\ . \tag{19}$$

In interpreting the above equation it is necessary to trace the path of the particle from its origin at $\mathbf{r}_i$ to its destination at $\mathbf{r}_{\mathcal{P}_i}$ a "time" β later and note how many times periodic boundary conditions have been invoked. This is analogous to determining the actual trajectory of a particle in a classical molecular-dynamics simulation using periodic boundary conditions. The winding number just describes the net number of times the paths of the N particles have wound around the periodic cell.

The free energy change, ΔF_v, is obtained from the winding-number distribution as

$$e^{-\beta\Delta F_v}=\frac{\int\rho_{\mathbf{v}}(R,R;\beta)dR}{\int\rho_{\mathbf{v}=0}(R,R;\beta)dR}=\langle e^{i(m/\hbar)\mathbf{v}\cdot\mathbf{W}L}\rangle\ . \tag{20}$$

The free-energy change is thus the Fourier transform of the winding-number distribution and is periodic under $v\rightarrow v+h/mL$. For small velocities

$$\beta\Delta F_v=\frac{m^2v^2}{2\hbar^2}\frac{\langle W^2\rangle L^2}{3}+O(v^4) \tag{21}$$

for a three-dimensional system assuming a cubic periodic cell. Comparison with Eq. (13) gives

$$\frac{\rho_S}{\rho}=\frac{m}{\hbar^2}\frac{\langle W^2\rangle L^2}{3\beta N}\ . \tag{22}$$

The mean-squared winding number can be related to the helicity modulus, Υ, introduced[5] to describe the free-energy change associated with "twisting the order parameter." Specifically, the helicity modulus was defined by fixing the order parameter at θ and 0 at opposite ends of a cylinder of area A and length L by the imposition of a wall potential and taking

$$\Upsilon=\lim_{A,L\rightarrow\infty}\left[-\frac{2L}{\theta^2A\beta}\ln\left[\frac{Z_\theta}{Z_0}\right]\right]\ , \tag{23}$$

where Z is the partition function. This prescription can be made precise following the above discussion. If this cylindrical system is made periodic in the L direction, then moving the walls with a velocity v is equivalent to a phase factor $\theta=mvL/\hbar$ and, from Eqs. (20) and (23),

$$\Upsilon=-\frac{2L}{\theta^2A\beta}\ln\langle e^{i\theta W}\rangle=\frac{L\langle W^2\rangle}{A\beta}\ , \tag{24}$$

where the last equality is in the limit of small v or θ, and W here refers to the winding number in the L direction.

Nothing in the above derivation is restricted to three dimensions and, in general, for dimensionality d,

$$\frac{\rho_S}{\rho}=\frac{m}{\hbar^2}\frac{\langle W^2\rangle L^{2-d}}{\rho\, d\beta}\ . \tag{25}$$

It has been predicted theoretically[6] and observed experimentally[7] that for ^{4}He films the superfluid density jumps from 0 to the universal value

$$\rho_S(T_c^-)=\frac{2}{\pi}\frac{mk_BT_c^-}{\hbar^2} \tag{26}$$

just below the transition. In the present language this says that the average squared winding number, $\langle W^2\rangle$, jumps from 0 to $4/\pi$ just below the transition, independent of particle density and periodic cell size. In this paper only three-dimensional simulations are reported.

The expression for the superfluid fraction can be rewritten as the ratio of two "diffusion" constants,

$$\frac{\rho_S}{\rho}=\frac{D_p}{D_0}\ , \tag{27}$$

where $D_0\equiv\hbar^2/2m$ is the usual quantum "diffusion" constant and D_p is a permutation partner "diffusion" constant,

$$D_p\equiv\frac{1}{N}\left\langle\left[\sum_{i=1}^{N}\mathbf{r}_i-\mathbf{r}_{\mathcal{P}_i}\right]^2\right\rangle\Big/2d\beta\ , \tag{28}$$

analogous to the Einstein expression for self-diffusion in a classical fluid ($D=\langle x^2\rangle/2t$).

Accurate computation of the mean-squared winding number is difficult since a change in, for example, W_x, involves a "global move." This is because W_x is a topological characteristic of the path. In the $\tau\rightarrow0$ limit the paths become continuous directed closed loops on a torus. W_x equals the number of paths intersecting a y-z plane going in the $+x$ direction minus the number intersecting this plane going in the $-x$ direction and is invariant to which cross section one takes. Hence, to change the winding number an entire path across the periodic cell must be changed. The number of atoms involved in a winding-number change will be at least proportional to the length of the central periodic cell. A practical consequence of this is that the algorithm used here, which was not developed with winding numbers in mind, converges somewhat slowly.

B. Relationship to the MDCF

A more detailed description of superfluidity is given by the momentum-density correlation function which

enters in the linear-response treatment of boundary motion. Expanding $\rho_{\mathbf{v}}$ in Eq. (9) to first order in v gives

$$\frac{\rho_N}{\rho} Nm\mathbf{v} = \langle \mathbf{P} \rangle_{\mathbf{v}} = \beta \langle \mathbf{PP} \rangle \cdot \mathbf{v} \ , \tag{29}$$

or, for an isotropic system in d dimensions,

$$\frac{\rho_N}{\rho} = \frac{\langle P^2 \rangle}{dNmk_B T} \ . \tag{30}$$

This expansion assumes H to be translationally invariant along the direction of $\mathbf{P}$ so that H and $\mathbf{P}$ commute. The more general case of, for example, a closed system where H might include an external potential representing the boundaries and thus not commute with $\mathbf{P}$, is also easily handled in path-integral computations (see Appendix).

For a classical fluid only the self-terms in $\langle P^2 \rangle$ are nonzero and are proportional to the kinetic energy, and thus $\rho_N = \rho$. In a superfluid $\rho_N < \rho$ because of the negative non-self-momentum correlations, as will be explicitly shown by the computations.

Evaluating Eq. (30) for the free-particle density matrix [the first product in Eq. (3)] reproduces the winding-number expression given earlier in Eq. (22). This derivation is, in fact, true, in general, since in the density matrix for an interacting system everything except the one-body or free-particle terms depend on the relative coordinates and are thus unaffected by a translation (generated by the total-momentum operator). Repeating this remark more explicitly, apply the total-momentum operator, $\mathbf{P} = -i\hbar \sum_j \nabla_j$, to the density matrix as given by Eqs. (2) and (3). The pair term in (3) is not affected since it depends only on the relative coordinates. Equation (22) follows, with, of course, the expectation computed using the full rather than just the free-particle density matrix.

Repeating Eq. (29) for the momentum-density, $\mathbf{p}(\mathbf{r})$, response yields

$$\langle \mathbf{p}(\mathbf{r}) \rangle_V = \beta \int_\Omega \langle \mathbf{p}(\mathbf{r}) \mathbf{p}(\mathbf{r}') \rangle_0 d\mathbf{r}'^3 \cdot \mathbf{V} \ , \tag{31}$$

where the total momentum has been written as the integral of the momentum density over the system volume Ω. The MDCF is thus the response function relating the expected momentum density to the motion of the sample boundaries.

An extensive discussion and proof of the properties stated below for this correlation function may be found in Refs. 3 and 4. The expected momentum response to motion of the sample walls depends on the boundary conditions. For a closed sample the entire fluid responds, while for a system with periodic boundary conditions only the normal component responds. The integral in Eq. (31) thus depends on the sample boundaries when $\rho_n \neq \rho$. The integrand (the MDCF) must therefore be long ranged, i.e., decays as slowly as $1/r^3$—but no slower or there would also be a volume dependence when the superfluid density is nonzero.

In an isotropic liquid the momentum-density correlation function can be written in the form

$$\overleftrightarrow{G}(\mathbf{r}) \equiv \langle \mathbf{p}(\mathbf{r}) \mathbf{p}(0) \rangle = [\tfrac{2}{3} m\rho K \delta(r) + G_N(r)] \overleftrightarrow{I} + G_S(r) \frac{3\hat{r}\hat{r} - \overleftrightarrow{I}}{r^3} \ , \tag{32}$$

since the only available second-rank tensors are $\hat{r}\hat{r}$ and $\overleftrightarrow{I}$. This defines the two functions $G_N(r)$ and $G_S(r)$. K is the kinetic energy per particle.

$G_N(r)$ and $G_S(r)$ have the important properties that

$$\rho_N = \rho \left[\tfrac{2}{3}\beta K + \int_0^\infty 4\pi\rho r^2 \frac{G_N(r)}{mk_B T \rho^2} dr \right] = \frac{\beta}{3m} \int \langle \mathbf{p}(\mathbf{r}) \cdot \mathbf{p}(0) \rangle d^3 r \ , \tag{33}$$

and for periodic boundary conditions,

$$G_S(r) \to -\frac{\rho_S m k_B T}{4\pi} \tag{34}$$

at large r, which can be used to compute normal and superfluid densities. Equation (33) is equivalent to Eq. (29). Equation (34) follows from the f-sum rule[4] and will be demonstrated for the ideal and the weakly interacting Bose gas in the next section. First, explicit formulas for the MDCF will be derived.

Using the form for the momentum-density operator in coordinate space,

$$\mathbf{p}(\mathbf{r}) = \frac{\hbar}{2i} \sum_j \nabla_j \delta(\mathbf{r} - \mathbf{r}_j) + \delta(\mathbf{r} - \mathbf{r}_j) \nabla_j \ , \tag{35}$$

the ensemble average in Eq. (32) may be written as

$$\langle \mathbf{p}(\mathbf{r}_1) \mathbf{p}(\mathbf{r}_2) \rangle = -\frac{\hbar^2}{4} \lim_{\substack{1' \to 1 \\ 2' \to 2}} (\nabla_1 - \nabla_{1'})(\nabla_2 - \nabla_{2'}) \times n^{[2]}(12, 1'2'; \beta) \ , \tag{36}$$

where the two-particle density matrix,

$$n^{[2]}(12, 1'2'; \beta) \equiv \frac{N(N-1) \int \rho(1, 2, 3, \ldots, N, 1', 2', 3, \ldots, N; \beta) d3 \cdots dN}{e^{-\beta F}} \ , \tag{37}$$

in terms of the N-body density matrix.

Using Eqs. (36), (3), and (4) the MDCF has the explicit form

$$\overleftrightarrow{G}(\mathbf{r}) = -\frac{\hbar^2 \rho}{4} \left\langle \frac{1}{N} \sum_{i,j} [\mathcal{F}_i \mathcal{F}_j - \nabla_i \nabla_j U(\mathbf{r}_{ij}^{[1]}, \mathbf{r}_{ij}^{[2]}; \tau) - \nabla_i \nabla_j U(\mathbf{r}_{\rho_i \rho_j}^{[M]}, \mathbf{r}_{ij}^{[1]}; \tau)] \delta(\mathbf{r} - \mathbf{r}_{ij}^{[1]}) \right\rangle \ , \tag{38}$$

where

$$\mathcal{F}_i=\frac{\mathbf{r}_i^{[2]}-\mathbf{r}_{\mathcal{P}_i}^{[M]}}{\hbar^2\tau/m}-\sum_l \nabla_i U(\mathbf{r}_{il}^{[1]},\mathbf{r}_{il}^{[2]};\tau)$$

$$+\sum_l \nabla_i U(\mathbf{r}_{\mathcal{P}_i\mathcal{P}_l}^{[M]},\mathbf{r}_{il}^{[1]};\tau)\ . \tag{39}$$

The $\langle\ \rangle$ here denotes averaging with the density matrix of Eq. 3 and over permutations, which are written as $\mathcal{P}$ in the above equations. The superscripts refer to points along the discretized path of the particle indicated by the subscript. All gradients are with respect to $r^{[1]}$.

For sufficiently small τ and "end-point" approximation

$$U(\mathbf{r},\mathbf{r}';\tau)=\tfrac{1}{2}[U_0(r;\tau)+U_0(r';\tau)] \tag{40}$$

becomes accurate for the pair density matrix. If this approximation is used, Eqs. (38) and (39) simplify considerably. Only the first term, the free-particle part, remains in the expression for $\mathcal{F}$, and the last two terms in Eq. (38), which are short ranged, may now be evaluated using the radial distribution function. The interesting part of the MDCF is thus just the correlation between "steps" separated by $\mathbf{r}$ along the paths in the path integrals. The presence of a superfluid fraction thus corresponds to a "dipolarlike" correlation in these paths at large r because the paths are winding around the torus.

Three ways of estimating the superfluid fraction have been introduced: Eqs. (22), (33), and (34). The variance of all three estimators is probably controlled by the slow convergence of the winding-number distribution. The winding-number estimator, Eq. (22), has the significant advantage that it does not explicitly contain the "time step" τ, while the variance of $\vec{G}$ diverges as $\tau\to 0$. Thus for sufficiently small τ the estimator based on the winding number will have less statistical uncertainty.

IV. APPLICATION TO IDEAL AND WEAKLY INTERACTING BOSE GASES

The MDCF can be easily evaluated for the ideal Bose or Fermi gas since in the grand-canonical ensemble the two-particle density matrix factorizes into a direct and an exchange term,

$$n^{[2]}(12,1'2')=n^{[1]}(11')n^{[1]}(22')\pm n^{[1]}(12')n^{[1]}(21')\ , \tag{41}$$

where the upper sign is for bosons and the lower for fermions. For any system the one-particle density matrix is the transform of the single-particle momentum distribution

$$n^{[1]}(r)=n_0+\int n(k)e^{i\mathbf{k}\cdot\mathbf{r}}\frac{dk^3}{(2\pi)^3}\ , \tag{42}$$

where n_0 is the condensate fraction. Using Eqs. (33), (36), (41), and (42) with the ideal-gas momentum distribution correctly reproduces the ideal-gas result,

$$\rho_n=\frac{\beta\hbar^2}{3m}\int k^2 n(k)[1\pm n(k)]\frac{dk^3}{(2\pi)^3}$$

$$=\frac{\hbar^2}{6m\pi^2}\int_0^\infty k^4\left[-\frac{\partial n(k)}{\partial\epsilon(k)}\right]dk$$

$$=\rho-n_0\ . \tag{43}$$

where $\epsilon(k)=\hbar^2k^2/2m$.

From the small-k behavior of the ideal Bose gas $n(k)$,

$$n(k)=\frac{1}{e^{\beta(\hbar^2k^2/2m-\mu)}-1}$$

$$=\frac{1}{(e^{-\beta\mu}-1)+(\hbar^2k^2/2m)e^{-\beta\mu}}+O(k^4)\ . \tag{44}$$

Equation (42) shows that above the transition temperature the one-particle density matrix falls off exponentially and thus so does $G_S(r)$. Below T_λ, where the chemical potential μ is zero,

$$n^{[1]}(r)\to n_0+\frac{m}{2\pi\beta\hbar^2}\frac{1}{r} \tag{45}$$

at large r. Together with Eqs. (36) and (41), this gives Eq. (34) with $\rho_S=n_0$.

Turning now to the weakly interacting case, the single-particle momentum distribution[8] leads to the large-r limit,

$$n^{[1]}(r)\to n_0+\frac{m}{4\pi\beta\hbar^2}\frac{1}{r}\quad\text{for } r\gg\beta\hbar c\ , \tag{46}$$

where c is the speed of sound. The large-r form is thus predicted to hold at distances such that phonons of the corresponding wavelength can be thermally excited. This distance is about 8.5 Å for ^{4}He at $T=2.0$ K and saturated vapor pressure. (A similar limit is predicted for the strongly interacting case, but with the coefficient multiplied by n_0/ρ_S (Refs. 9 and 10). Although the coefficient of the $1/r$ term in the above equation is half that for the ideal gas, the two-particle density matrix now contains a compensating "anomalous" term in addition to the direct and exchange terms of Eq. (41). Again, Eqs. (33) and (34) can be shown to hold for the weakly interacting model.[11] For a strongly interacting Bose system such as ^{4}He, the only presently available technique for studying momentum correlations is computer simulation.

V. SIMULATION RESULTS FOR ^{4}He

The winding-number distribution and the MDCF were computed by path-integral methods for a model of ^{4}He where the atoms interact by the Aziz (HFDHE2) pair potential.[12] Periodic boundary conditions were used for all cases. The computations discussed below are for 64 and 125 particles in the periodic cell and typically take 10 or more hours of central-processing-unit time on a Cray-1 computer for each computation. Most of this time is spent in equilibrating and averaging over permutations as required in Eq. (6).

TABLE I. Experimental (Ref. 13) and computed superfluid fractions, based on Eq. (22). Simulation results are for 64 atoms in the periodic cell. The number density ρ is in units of 10^{22} cm^{-3}. The standard error in the last digit of the computed superfluid fraction is given in parentheses. $P(W_x)$ is the probability of a winding number W_x in the x direction, and $P(W_x)=P(-W_x)$.

T (K)	ρ	ρ_S/ρ (expt.)	ρ_S/ρ	$P(0)$	$P(1)$	$P(2)$	$P(3)$	$P(4)$	$P(5)$	$P(6)$
2.86	2.142	0.0	0.03(1)	0.966	0.0168	0.0004				
2.50	2.179	0.0	0.08(2)	0.881	0.0582	0.0013				
2.35	2.191	0.0	0.16(2)	0.785	0.102	0.0055	0.0006			
2.00	2.191	0.45	0.44(4)	0.489	0.211	0.040	0.0046			
1.82	2.186	0.66	0.66(4)	0.352	0.233	0.077	0.013	0.002		
1.60	2.183	0.83	0.88(7)	0.270	0.221	0.107	0.031	0.005	0.0009	0.0002
1.18	2.182	0.98	0.98(5)	0.223	0.195	0.118	0.052	0.018	0.005	0.001

Earlier work[2] showed that using the full pair density matrix in Eq. (3) rather than the "end-point" approximation permitted much larger values of τ to be used without loss of accuracy in computing expectations such as the kinetic energy. For τ corresponding to 40 K (the value used for most of these computations) using the end-point approximation causes an error of about 8% in the kinetic energy and 1% or 2% in the potential energy. In these initial computations we have, however, used the end-point approximation in evaluating $\overleftrightarrow{G}$ [using Eqs. (38) and (39)], but retained the full pair density matrix in selecting the configurations and thus in computing the winding number.

Winding-number distributions and superfluid fractions for a series of simulations using 64 atoms in the central periodic cell are summarized in Table I. At the lowest temperature the winding-number distribution is Gaussian, while above T_λ it appears to be exponential. The computed superfluid fraction is in good agreement with experiment[13] well below the transition.

This is more clearly seen in Fig. 1, which compares ρ_N/ρ values computed from the integral of the MDCF [Eq. (33)] and from the winding number [Eq. (22)] with experiment.[13] All of the ρ_N/ρ estimates based on Eq. (33) shown there are for periodic systems of 125 atoms. Statistical uncertainties are estimated as roughly 10% for the estimates based on Eq. (33) and are indicated for the estimates based on the winding number. There is, in addition, the systematic error due to finite sample size. Finite-size effects have not been thoroughly studied here, but intuitively cause the transition to be rounded and displaced to higher temperatures since at all temperatures there is a nonzero probability of a path winding itself around a finite-size periodic cell, giving $\rho_S>0$. The winding-number distributions (here for the x direction) $P(W_x)$ are shown for two temperatures whose ρ_N/ρ values are given on the lower graph. These distributions, of course, depend on the periodic cell size.

Figure 2 shows the MDCF at $T=2.5$ K and $\rho=0.0218$ atoms/Å^3 for a system of 125 atoms in the periodic cell. This is well above the λ transition temperature of $T_\lambda=2.17$ K. To provide a convenient scale of distances, Fig. 2(a) shows the radial distribution function for this system. From Fig. 2(b), $G_N(r)$ is almost negligible except for nearest neighbors. Since the square-bracketed quantity in Eq. (33) must be less than 1 ($\rho_N\le\rho$), and the first term, the ratio of the correct quantum-mechanical kinetic energy to its classical value, is greater than 1, the integral involving $G_N(r)$ (dashed line) must be negative, as it is seen to be in Fig. 1(b). Accurate values for the kinetic energy along the saturated-vapor-pressure curve are given in Ref. 2. The error due to the use in the present work of the "end-point" approximation for τ of $\frac{1}{40}$ K increases these values by about 1.2 K. The value of ρ_N/ρ calculated from Eq. (33) using the $\tilde{G}_N(r)$ displayed in Fig. 2(a) is

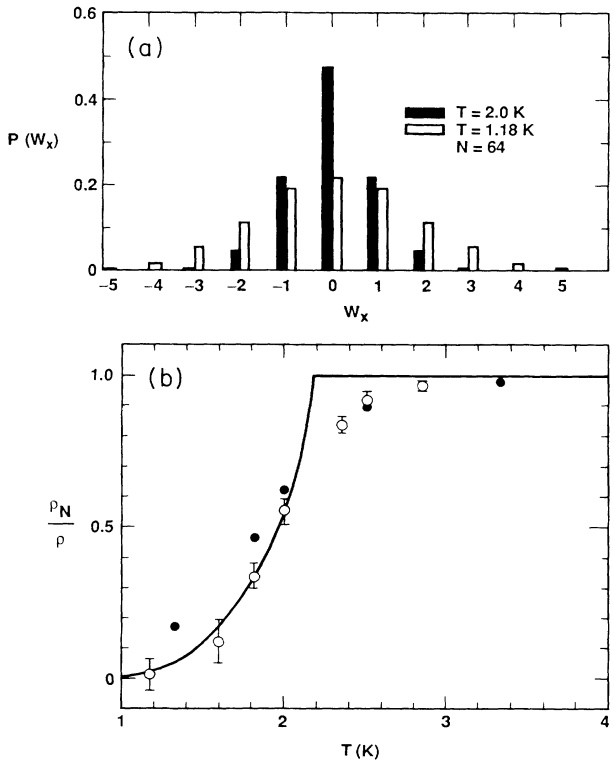

FIG. 1. Computed ρ_N/ρ values along the SVP curve (lower panel). The solid line is the experimental curve (Ref. 13). The solid dots, for 125 atoms, are calculated from Eq. (33). The estimates based on the winding number [Eq. (22)] (open circles) are for 64 atoms. The upper panel shows the x-direction winding-number distribution at $T=2.0$ and 1.18 K.

~ 0.9, with an estimated error of at least 10%. It is difficult to determine ρ_S from the asymptotic behavior of $G_S(r)$, Fig. 2(c), but it is consistent with $\rho_S \sim 0$.

Results for a system well below the λ transition are shown in Fig. 3 ($T=1.1765$ K, $\rho=0.0218$ atoms/Å^3, and 125 atoms in the periodic cell). As discussed in Ref. 2, it is much easier to do path-integral simulations for distinguishable particles than for bosons since averaging over permutations is not necessary. This is a luxury not available in real experiments. Results for both bosons (circles) and distinguishable particles (solid line) are compared in Fig. 3. The values for $G_N(r)$ are altered only

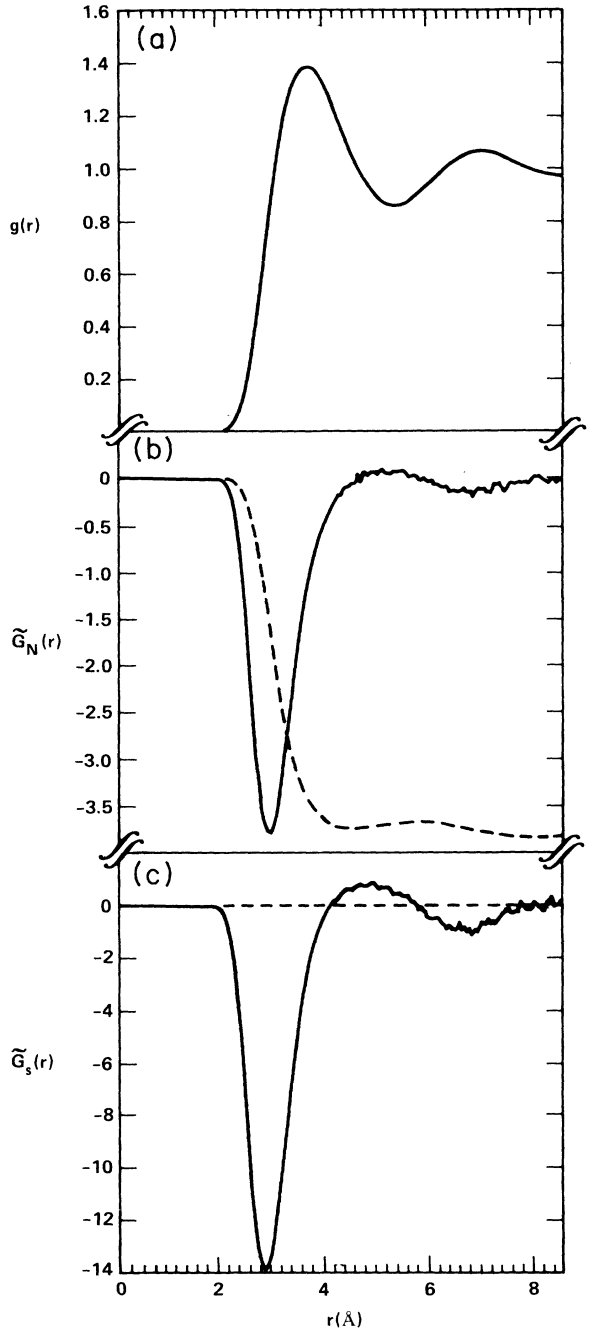

FIG. 2. Radial distribution function (top panel) and components of the MDCF, $\tilde{G}_N(r) \equiv 4\pi\rho r^2[G_N(r)/mk_BT\rho^2]$ (solid line, middle panel) in Å^{-1} and its integral (dashed line, middle panel), and $\tilde{G}_S(r) \equiv 4\pi\rho[G_S(r)/mk_BT\rho^2]$ (bottom panel) at $T=2.5$ K along the saturated vapor pressure (SVP) curve for $N=125$ particles in the periodic cell. $G_N(r)$ and $G_S(r)$ are defined in Eq. (32).

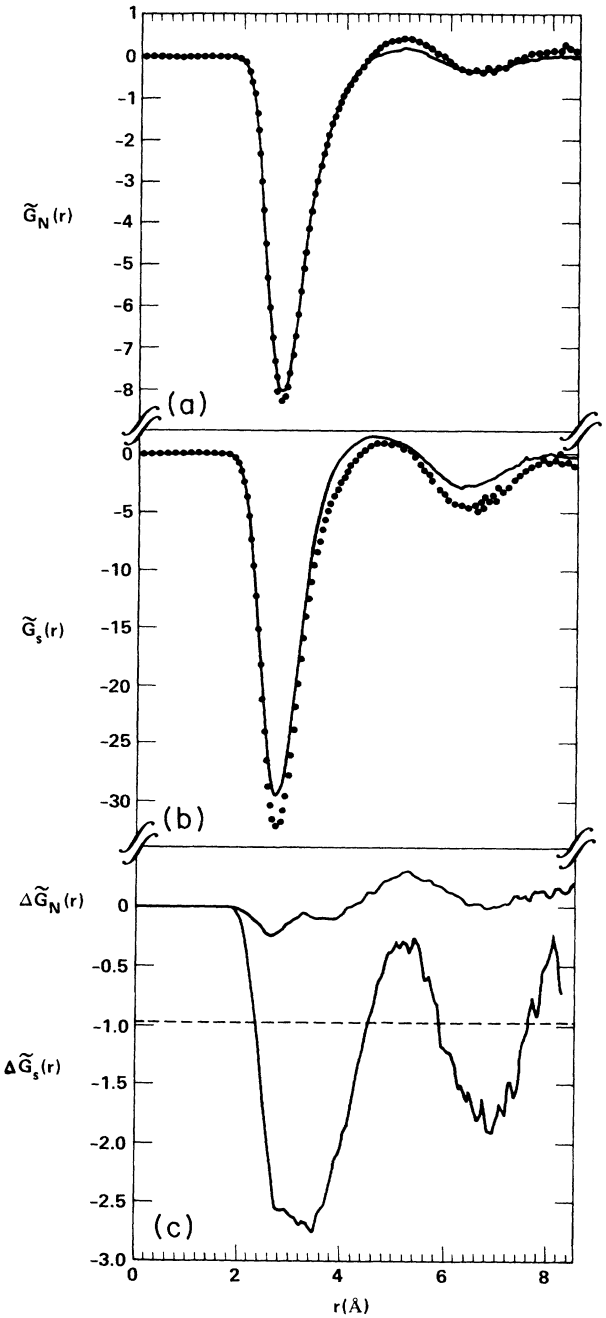

FIG. 3. $\tilde{G}_N(r)$ (top panel) and $\tilde{G}_S(r)$ (middle panel) at $T=1.18$ K and SVP. The solid lines are for distinguishable particles and the dots for bosons. The two curves in the bottom panel are the difference between the distinguishable-particle and the boson results. The dashed line is the experimental value for $-\rho_S/\rho$, the asymptotic limit of $\tilde{G}_S(r)$.

slightly by Bose statistics. The values of ρ_N/ρ calculated from Eq. (33) are 0.99 for the distinguishable-particle case and 0.20 for bosons. (The experimental value is 0.024.) Over 90% of this difference in ρ_N/ρ between bosons and distinguishable-particles is due to the kinetic energy difference rather than differences in $G_N(r)$. It is clear, however, that $G_N(r)$ has some dependence on statistics. For example, above T_λ, ρ_N/ρ is 1 for both cases, but the kinetic energy for the distinguishable-particle system is still larger than for the Bose system. This must be compensated by differences in the integral involving $G_N(r)$ in Eq. (33). The change in $G_S(r)$, Fig. 3(b), is a systematic lowering for the Bose case. The differences are plotted in Fig. 3(c). The $G_N(r)$ values (upper curve), as remarked above, are not significantly changed by Bose statistics; however, the subtraction process removes much of the short-range structure from $G_S(r)$ (lower curve), making it easier to determine the asymptotic limit for the Bose case. This asymptotic limit is still uncertain; however, it is definitely consistent with the experimental value of $\rho_S/\rho=0.976$ (dashed line).

Figure 4 displays the (equal-time) momentum correlations $\overleftrightarrow{G}(\mathbf{r})$ for $\mathbf{r}$ in the (x,y) plane for the boson case shown in Fig. 3. The vector-field components are proportional to

$$r^3(\langle p_x(\mathbf{r})p_x(0)\rangle,\ \langle p_y(\mathbf{r})p_x(0)\rangle)/mk_BT\rho^2 .$$

(The singular self-contribution at the origin is not indicated and some of the vectors at small r have been truncated for display purposes.) The distinguishable-particle case would be quite similar, but without the weak dipolar field at large r. The negative-momentum correlation between neighboring particles is again evident. This figure has no classical analog. In particular, it should not be misinterpreted as the flow field which develops at later times in response to the motion of a particle at the origin. That flow field, in contrast to Fig. 4, shows positive correlations between near-neighbor particles with a backflow at large distances. At low temperatures the density matrix becomes the product of the ground-state wave function at R and R'. If the ground-state wave function is approximated by the Jastrow form $\Psi_0=\exp(-\sum_{i<j}u_{ij})$, then

$$\overleftrightarrow{G}(r)=\frac{-\hbar^2}{2}\rho^2 g(r)\nabla\nabla u(r) , \tag{47}$$

which is in semiquantitative agreement with the short-range structure of $\overleftrightarrow{G}$ for the commonly used $u(r)$'s.[14]

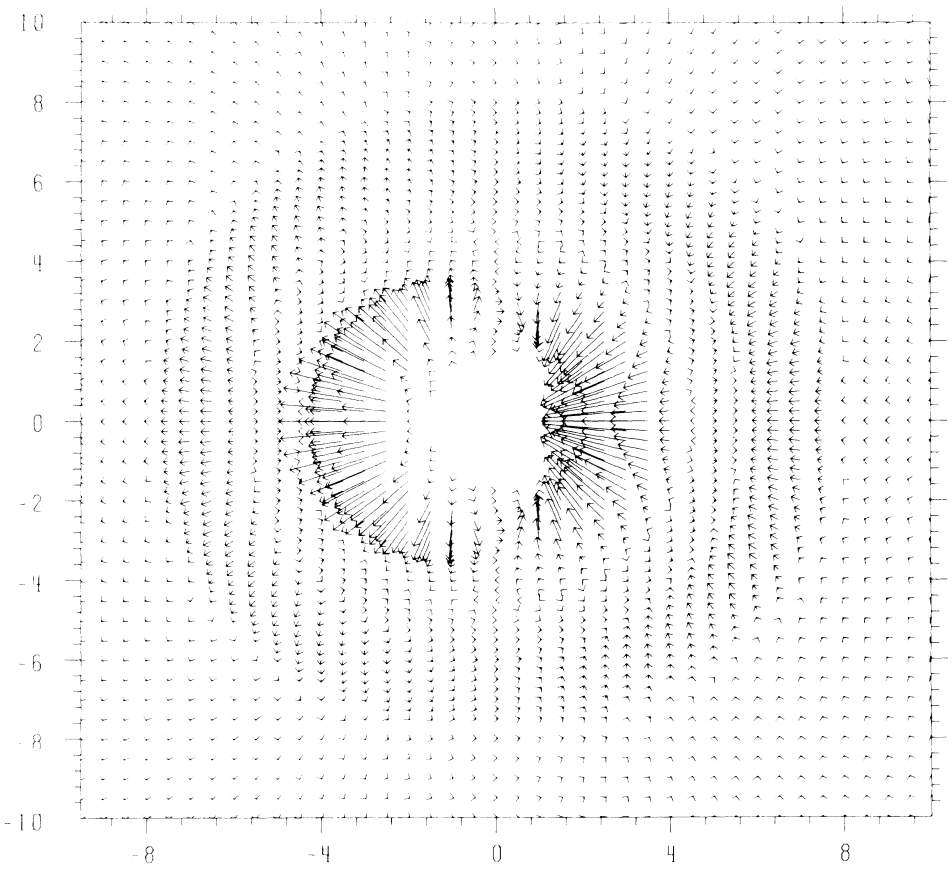

FIG. 4. Plot of $r^3[\overleftrightarrow{G}(\mathbf{r})/mk_BT\rho^2]$ for $T=1.18$ K and SVP. $\mathbf{r}$ is in the (x,y) plane and lengths are in Å. The self-term at the origin is not indicated.

VI. CONCLUSIONS

Several expressions for the superfluid density in the context of path-integral calculations have been given in this article: a new expression in terms of the topological concept of winding number in a periodic system and the equivalent formulation in terms of momentum correlations. These were demonstrated for ^{4}He. Winding-number calculations are the most convenient since little new analysis is required. Computations of the momentum correlation shown negative correlation between near neighbors and are consistent with an asymptotic decay proportional to the superfluid fraction times the inverse cube of the separation distance. Path-integral methods have now been used to compute both the momentum-condensate, specific heat and the superfluid fraction for the same model of ^{4}He. These calculations are computationally taxing, but this will be reduced by continuing algorithm development.

ACKNOWLEDGMENTS

This work was performed under the auspices of the U.S. Department of Energy by the Lawrence Livermore National Laboratory under Contract No. W-7405-ENG-48. We wish to thank several of our colleagues at Livermore, primarily B. J. Alder and John Garrison, and Eugene Loh, Jr. of University of California, Santa Barbara, and Los Alamos National Laboratory for helpful discussions and correspondence. We particularly thank Allan Griffin of the University of Toronto for his interest and aid in this research. Some of the computations reported here were done at the San Diego Supercomputer Center and at the National Center for Supercomputer Applications at the University of Illinois at Urbana-Champaign.

APPENDIX

If the system Hamiltonian is not translationally invariant, the momentum response of Eq. (29) must be calculated from the general linear-response formula

$$\langle \mathbf{P} \rangle_{\mathbf{v}} = \frac{1}{\mathcal{Z}} \mathrm{Tr} \left[\int_0^\beta d\lambda \, \mathbf{P} e^{-(\beta-\lambda)H} \mathbf{P} e^{-\lambda H} \right] \cdot \mathbf{v} \ , \tag{A1}$$

where $\mathbf{P}$ is the total-momentum operator and $\mathcal{Z} = \mathrm{Tr}[e^{-\beta H}]$. It is shown here that this formula leads to the same expression for the superfluid fraction in terms of winding numbers as before.

Approximate the above integral by a sum and use Eq. (2) on $\rho(R,R';\beta-\lambda)$ and $\rho(R',R;\lambda)$ to obtain

$$\langle \mathbf{P} \rangle_{\mathbf{v}} = \lim_{M\to\infty} \tau \left\langle \frac{\mathbf{P}\rho(R_1,R_2;\tau)}{\rho(R_1,R_2;\tau)} \sum_{K=2}^{M} \frac{\mathbf{P}\rho(R_K,R_{K+1};\tau)}{\rho(R_K,R_{K+1};\tau)} + \frac{\mathbf{P}\mathbf{P}\rho(R_1,R_2;\tau)}{\rho(R_1,R_2;\tau)} \right\rangle \cdot \mathbf{v} \tag{A2}$$

where the angular brackets $\langle \ \rangle$ imply averaging over the distribution (including permutations $\mathcal{P}$)

$$\frac{1}{N!\mathcal{Z}} \prod_{i=1}^{M} \rho(R_i,R_{i+1};\tau) \ ,$$

with $R_{M+1} = \mathcal{P}R_1$ and $\tau = \beta/M$. In the limit of small τ,

$$\ln[\rho(R_K,R_{K+1};\tau)] = -\frac{(R_K-R_{K+1})^2}{2\hbar^2\tau/m} - \frac{\tau}{2}[V(R_K)+V(R_{K+1})] + O(\tau^2) \tag{A3}$$

where $V(R_K)$ is the total potential energy.

Using Eq. (50) in Eq. (49), applying the momentum operator, and symmetrizing over which point is labeled as the beginning of the path gives

$$\langle \mathbf{P} \rangle_{\mathbf{v}} = Nm\mathbf{v} + \left\langle -\frac{1}{\beta} \left[\frac{m}{\hbar} \mathbf{W}L + \tau \mathbf{F} \right] \times \left[\frac{m}{\hbar} \mathbf{W}L + \tau \mathbf{F} \right] + \tau \overleftrightarrow{\mathbf{K}} \right\rangle \cdot \mathbf{v} + O(\tau^2) \tag{A4}$$

where

$$\mathbf{W}L = \sum_{K=1}^{M} \sum_{i=1}^{N} (\mathbf{r}_i^{K+1} - \mathbf{r}_i^K) \tag{A5}$$

is proportional to the center-of-mass displacement around the path,

$$\mathbf{F} = \frac{\tau\hbar}{2} \sum_{K=1}^{M} \sum_{i=1}^{N} \nabla_i V(R_K) \tag{A6}$$

is proportional to the integrated force around the path, and

$$\overleftrightarrow{\mathbf{K}} = \frac{\tau\hbar^2}{2} \sum_{K=1}^{M} \sum_{i=1}^{N} \nabla_i \nabla_i V(R_K) \ . \tag{A7}$$

As $\tau \to 0$, $\mathbf{W}$, $\mathbf{F}$, and $\overleftrightarrow{\mathbf{K}}$ approach a constant for any given path. Terms proportional to τ drop out in the limit and

$$\langle \mathbf{P} \rangle_{\mathbf{v}} = Nm\mathbf{v} - \frac{m^2}{\beta\hbar^2} \langle \mathbf{W}\mathbf{W} \rangle \cdot \mathbf{v} \ . \tag{A8}$$

For a liquid, $\langle \mathbf{W}\mathbf{W} \rangle$ will be diagonal and the momentum response will be along $\mathbf{v}$.

As before, the normal fraction is defined as that part of the liquid which moves with the side walls,

$$\langle \mathbf{P} \rangle_{\mathbf{v}} = \frac{\rho_N}{\rho} Nm\mathbf{v} \ ; \tag{A9}$$

hence,

$$\frac{\rho_N}{\rho} = 1 - \frac{m\langle W_x^2 \rangle L^2}{\beta\hbar^2 N} \ . \tag{A10}$$

[1]For an introduction to path integrals and to superfluid ^{4}He, see R. P. Feynman, *Statistical Mechanics* (Benjamin, Reading, MA, 1972).

[2]E. L. Pollock and D. M. Ceperley, Phys. Rev. B **30**, 2555, (1984); D. M. Ceperley and E. L. Pollock, Phys. Rev. Lett. **56**, 351 (1986); D. M. Ceperley and E. L. Pollock, Can. J. Phys. (to be published).

[3]P. C. Hohenberg and P. C. Martin, Ann. Phys. (N.Y.) **34**, 291 (1965). Earlier references may also be found there.

[4]G. Baym, in *Mathematical Methods in Solid State and Superfluid Theory,* edited by R. C. Clark and G. H. Derrick (Oliver and Boyd, Edinburgh, 1969), p. 121. See also D. Forster, *Hydrodynamic Fluctuations, Broken Symmetry, and Correlation Functions* (Benjamin/Cummings, Reading, MA, 1975).

[5]M. E. Fisher, M. N. Barber, and D. Jasnow, Phys. Rev. A **8**, 1111 (1973).

[6]D. R. Nelson and J. M. Kosterlitz, Phys. Rev. Lett. **39**, 1201 (1977).

[7]D. J. Bishop and J. D. Reppy, Phys. Rev. Lett. **40**, 1727 (1978).

[8]A. A. Abrikosov, L. P. Gor'kov, and I. E. Dzyaloshinski, *Methods of Quantum Field Theory in Statistical Physics* (Dover, New York, 1963), 36.

[9]N. N. Bogoliubov, *Lectures on Quantum Statistics* (Gordon and Breach, New York, 1970), Vol. 2.

[10]A. Griffin, Phys. Rev. B **30**, 5057 (1984), Eqs. (31) and (32).

[11]Details may be found in A. Griffin and E. Talbot [Phys. Rev. B **24**, 5075 (1981)] and Alexander L. Fetter [Ann. Phys. (N.Y.) **60**, 464 (1970) Eqs. 36–45].

[12]R. A. Aziz, V. P. S. Nain, J. S. Carley, W. L. Taylor, and G. T. McConville, J. Chem. Phys. **70**, 4330 (1979).

[13]R. J. Donnelly, *Experimental Superfluidity* (The University of Chicago Press, Chicago, 1967), Table 14.

[14]W. L. McMillan, Phys. Rev. **138**, A422 (1965).